

# THE PROBABILITY DISTRIBUTION FUNCTION OF THE SZ POWER SPECTRUM: AN ANALYTICAL APPROACH

PENGJIE ZHANG

Shanghai Astronomical Observatory, Chinese Academy of Science, 80 Nandan Road, Shanghai, China, 200030 and  
Joint Institute for Galaxy and Cosmology (JOINGC) of SHAO and USTC

RAVI K. SHETH

209 S. 33rd Street, Department of Physics and Astronomy, University of Pennsylvania, Philadelphia, PA 19104, USA  
*Draft version September 27, 2018*

## ABSTRACT

The Sunyaev Zel'dovich (SZ) signal is highly non-Gaussian, so the SZ power spectrum (along with the mean  $y$  parameter) does not provide a complete description of the SZ effect. Therefore, SZ-based constraints on cosmological parameters and on cluster gas physics which assume Gaussianity will be biased. We derive an analytic expression for the  $n$ -point joint PDF of the SZ power spectrum. Our derivation, which is based on the halo model, has several advantages: it is expressed in an integral form which allows quick computation; it is applicable to any given survey and any given angular scale; it is straightforward to incorporate many of the complexities which arise when modeling the SZ signal. To illustrate, we use our expression to estimate  $p(C_\ell)$ , the one-point PDF of the SZ power spectrum. For small sky coverage (applicable to BIMA/CBI and the Sunyaev Zel'dovich Array experiments), our analysis shows that  $p(C_\ell)$  on the several arc-minute scale is expected to be strongly skewed, peaking at a value well below the mean and with a long tail which extends to tail high  $C_\ell$  values. In the limit of large sky coverage (applicable to the South Pole Telescope and Planck),  $p(C_\ell)$  approaches a Gaussian form. However, even in this limit, the variance of the power spectrum is very different from the naive Gaussian-based estimate. This is because different  $\ell$  models are strongly correlated, making the cosmic variance of the SZ band-power much larger than the naive estimate. Our analysis should also be useful for modeling the PDF of the power spectrum induced by gravitational lensing at large  $\ell$ .

*Subject headings:* Cosmology: theory-large scale structure-cosmic microwave background-methods: statistical

## 1. INTRODUCTION

The Sunyaev Zel'dovich (SZ) effect (Zeldovich & Sunyaev 1969; Sunyaev & Zeldovich 1972) is a powerful probe of baryons, dark matter and dark energy (Birkinshaw 1999; Carlstrom et al. 2002). To extract the full statistical power of this probe, SZ statistics must be understood to an accuracy which matches that which the observations will reach. The statistic which has been most actively studied is the ensemble average power spectrum  $\bar{C}_\ell$  of the thermal SZ signal. For the simplest case of adiabatic gas evolution, both analytic (Cole & Kaiser 1988; Makino & Suto 1993; Atrio-Barandela & Mucket 1999; Komatsu & Kitayama 1999; Molnar & Birkinshaw 2000; Majumdar 2001; Zhang & Pen 2001; Komatsu & Seljak 2002) and numerical (da Silva et al. 2000; Refregier et al. 2000; Seljak, Burwell & Pen 2001; Springel, White & Hernquist 2001; Zhang, Pen & Wang 2002) approaches are beginning to give consistent results (Refregier & Teyssier 2002; Komatsu & Seljak 2002).

However,  $\bar{C}_\ell$  alone (or in combination with the mean  $y$  parameter) does not provide a complete description of the SZ effect. This is because the SZ signal is strongly non-Gaussian (Cooray 2001; Seljak, Burwell & Pen 2001; Yoshida, Sheth & Diaferio 2001; Zhang, Pen & Wang 2002; Komatsu & Seljak

2002). In contrast to the primary CMB and weak gravitational lensing signals, the SZ signal is non-Gaussian even on large scales (Zhang & Pen 2001). This is because the effect is dominated by rare massive clusters. Therefore, interpretation of a SZ  $C_\ell$  measurement requires not only a robust prediction of the expected ensemble-averaged  $\bar{C}_\ell$ , but also the probability distribution function (PDF) of  $C_\ell$  around this mean value.

Because the SZ effect is dominated by the most massive clusters, and the abundance of such clusters is very sensitive to the amplitude of density fluctuations (Press & Schechter 1974; Sheth & Tormen 1999), the SZ power spectrum depends strongly on  $\sigma_8$ :  $C_l \propto \sigma_8^{\sim 7}$  for the range of currently interesting cosmological models (Seljak, Burwell & Pen 2001; Zhang & Pen 2001; Komatsu & Seljak 2002). In principle, this makes the SZ power spectrum a powerful probe of  $\sigma_8$ . The CMB power spectra excess reported by CBI (Mason et al. 2003; Readhead et al. 2004) and BIMA (Dawson et al. 2002) are consistent with having a contribution from the SZ effect provided  $\sigma_8 \simeq 1.0$  (Dawson et al. 2002; Bond et al. 2005; Readhead et al. 2004). This SZ explanation is further supported by the frequency dependence of the CMB power excess (Kuo et al. 2006). However, this value is uncomfortably high compared to the WMAP3 value of  $\sigma_8 \approx 0.8$  (Spergel et al. 2006).

The SZ-based estimates of  $\sigma_8$  assume adiabatic evolution of the gas. Feedback (da Silva et al. 2001;

White, Hernquist & Spingel 2002; Lin et al. 2004) and cooling (da Silva et al. 2001; Zhang & Wu 2003) effects can decrease the SZ power spectrum by a factor of 2; if these are included, then the required value of  $\sigma_8$  increases further. Other mechanisms such as magnetic fields (Zhang 2004) can further reduce the amplitude of  $C_\ell$ . Other contributions to the SZ signal have also been studied—the SZ effect of the first stars (Oh et al. 2003), and contributions from unvirialized intergalactic medium (Atrio-Barandela & Mucket 2006). But if the WMAP 3 estimates are accurate,  $\tau \simeq 0.1$  and  $\sigma_8 \simeq 0.8$ , then these additional contributions are likely to be subdominant. Thus to explain the CBI/BIMA SZ measurements it appears that  $\sigma_8 \gtrsim 1.1$ – $1.2$ : evidently, a severe discrepancy with the CMB-based estimate exists<sup>1</sup>.

There are at least two ways in which the discrepancy can be decreased. One is to assume that the uncertainty on the estimate is artificially small. This would happen, for instance, if the statistical errors on the SZ  $C_\ell$  and  $C_{\ell'}$  are highly correlated, even for widely separated  $\ell, \ell'$  pairs. If so, then the cosmic variance of the measured band-power SZ  $C_\ell$  would be much larger than the naive Gaussian-based estimates.

Alternatively, the SZ-based estimates of  $\sigma_8$  arise from requiring the measured  $C_\ell$  to match the ensemble averaged power spectrum predicted from theory. However, if the distribution of  $C_\ell$  is skewed, then this requirement is unreasonable. Since we have good reason to expect the signal to be non-Gaussian, it may be that the discrepancy can be resolved if one accounts for this non-Gaussianity. For small sky coverage in particular,  $p(C_\ell)$  can be highly skewed, with a non-negligible tail toward high  $C_\ell$ . Thus, for a survey with small sky coverage, the probability of obtaining  $C_\ell$  several times larger the mean  $C_\ell$  is not negligible. Dawson et al. (2006) simulated an SZ map for one choice of cosmological model and then scaled the simulated SZ decrement (assuming the signal scales as  $\sigma_8^{7/2}$ , so that  $C_\ell$  scales as  $\sigma_8^7$ ) to estimate the effect of this non-Gaussianity as  $\sigma_8$  varies. They used this procedure to argue that  $\sigma_8 \sim 0.7$  may well produce a long enough tail of  $C_\ell$  values to explain the CBI/BIMA measurement. While this is reassuring, it is not obvious that this simple rescaling is indeed an accurate description of how the non-Gaussian distribution of  $C_\ell$  depends on  $\sigma_8$ .

The discussion above shows why understanding the full PDF of  $C_\ell$  is crucial. Current theoretical understanding of  $p(C_\ell)$  is limited. Even for a single cosmological model and a given sky coverage (e.g.  $1 \text{ deg}^2$  or larger), simulations lack sufficient realizations to measure the full PDF reliably. The scaling method of Dawson et al. (2006) only provides a crude estimate, since the non-Gaussianity (and the PDF) is certainly a function of  $\sigma_8$ . Analytical estimates of the low order moments of  $p(C_\ell)$ , such as the variance and covariance of  $C_\ell$  have been made (Cooray 2001; Zhang & Pen 2001; Komatsu & Seljak 2002). These calculations provide quantitative estimates of the errors in  $C_\ell$ , and represent important first steps towards understanding the SZ

non-Gaussianity. However, to specify  $p(C_\ell)$ , higher order moments are also required. The computational time required to calculate higher order moments rapidly becomes prohibitive. To estimate  $p(C_\ell)$  for any given cosmology and given survey strategy in a reasonable amount of time, going beyond this moment by moment calculation is essential.

This paper presents a fast, complete, analytical method for calculating the full  $n$ -point PDF. It is based on the halo model (Cooray & Sheth 2002) and allows one to easily estimate the effect on the SZ signal of different treatments of the relevant gas physics. §2 outlines the halo model calculation of the lowest order statistics of the SZ power spectrum: the mean, the variance and the covariance. An analytical expression for the  $n$ -point joint PDF of the SZ power spectrum is derived in §3. We show explicitly that it correctly reproduces the usual expressions for the mean, variance and covariance. We then show that the analysis is particularly simple in the limits of very large and very small sky coverage. A numerical calculation of the one-point PDF, and a comparison with the large sky coverage limit is presented in §3.6. §4 summarizes our results, highlights several key simplifications in our approach, and discusses possible extensions.

Where necessary in this paper, we adopt a flat  $\Lambda$ CDM cosmology with  $\Omega_m = 0.3$ ,  $\Omega_\Lambda = 0.7$ ,  $\sigma_8 = 0.9$ , and  $H_0 = 100h \text{ km s}^{-1} \text{ Mpc}^{-1}$  with  $h = 0.7$ . To illustrate our results we use an initial power spectrum with index  $n = 1$ , the BBKS fitting formula for the transfer function, the NFW profile (Navarro, Frenk & White 1996) for the dark matter profile, the Press-Schechter formula (Press & Schechter 1974) for the halo mass function and the associated halo bias factor (Mo & White 1996) when modeling halo clustering. When our formalism is used to interpret simulations or observations, more accurate models of halo abundance and clustering, such as those of Sheth & Tormen (1999), should be used.

## 2. THE MEAN, VARIANCE AND COVARIANCE OF THE SZ POWER SPECTRUM

The dominant contribution to the SZ power spectrum is from virialized regions (Seljak, Burwell & Pen 2001; White, Hernquist & Spingel 2002; Cooray & Sheth 2002; Hernandez-Monteagudo et al. 2006). This makes the halo model particularly well suited for estimating  $C_\ell$  and its distribution. On the angular scales of interest in what follows, the two-halo term is always much smaller than the one-halo term: the contribution is less than 1% at  $\ell \gtrsim 1000$  (Komatsu & Kitayama 1999), so it can be neglected. Thus, the measured power spectrum  $C \equiv C(\ell)|_S$  at multipole  $\ell$ , is just a sum over the contributions from each cluster in the survey. I.e., for a survey with sky coverage  $f_{\text{sky}}$ ,

$$C|_S = f_{\text{sky}}^{-1} \int dz \frac{dV}{dz} \int dM \frac{dn}{dM} S(M, z; \lambda) \rho(\lambda|M, z) d\lambda. \quad (1)$$

Here,  $V$  is the survey volume. The explicit factor  $f_{\text{sky}}^{-1}$  in the above equation cancels the implicit dependence of  $V$  on  $f_{\text{sky}}$  ( $V \propto f_{\text{sky}}$ ) so the expectation value of  $C|_S$  does not depend on  $f_{\text{sky}}$ .  $S(M, z; \lambda)$  is the SZ power spectrum of a single cluster at the corresponding  $\ell$ . In this and the following expressions, we assume that no confusion will arise from the fact that we do not write

<sup>1</sup> Contaminations of unresolved and unremoved point sources remain a possible solution to the power excess problem (White & Majumdar 2004; Toffolatti et al. 2005; Douspis et al. 2006), although current modeling is quite uncertain.

explicitly that both  $S$  and  $C$  depend on  $\ell$ . The quantity  $S$  describes the structure of the cluster; it is mainly determined by the cluster mass  $M$  and redshift  $z$ , but it also depends on other parameters  $\lambda$ , which may include the cluster concentration parameter  $c$ , cluster shape, etc. These parameters may or may not correlate tightly with  $M$ , and, in general, they almost certainly are not fixed by  $M$  alone. We use  $\rho(\lambda|M, z)$  to denote the distribution of these parameters at fixed  $M$  and  $z$ ; it is normalized so that  $\int \rho(\lambda|M, z) d\lambda = 1$ . For simplicity, we neglect these extra parameters in the numerical calculations which follow, although we do include them in our analytical expressions. We will discuss their possible effects later.

If  $d\bar{n}/dM$  is the ensemble averaged halo mass function, then the comoving number density of clusters per mass interval that are actually in the survey volume is

$$dn/dM = d\bar{n}/dM [1 + \delta_L(M) + \delta_P]. \quad (2)$$

Here,  $\delta_L(M)$  denotes the mean fluctuation in cluster number density which arises from the fact that the density of dark matter in the survey volume may not be exactly the same as the universal average, and  $\delta_P$  represents the fluctuation which arises from the fact that clusters represent a discrete point process realization of the smooth density field  $d\bar{n}/dM [1 + \delta_L(M)]$ . It is standard to assume that  $\delta_P$  is drawn from a Poisson distribution with mean  $d\bar{n}/dM [1 + \delta_L(M)]$  (Casas-Miranda et al. 2002; Hu & Cohn 2006; Holder 2006).

In what follows, we will often consider bins in redshift, mass and  $\lambda$ . We use the Latin letter  $j$  to denote  $j$ th redshift bin and the Greek letter  $\alpha$  to denote the  $\alpha$ th bin of  $M$  and  $\lambda$ . The expectation value of  $C|_S$  is

$$\bar{C} = \int dz \frac{dV^f}{dz} \int dM \frac{d\bar{n}}{dM} S(M, z; \lambda) \rho(\lambda|M, z) d\lambda, \quad (3)$$

where  $V^f$  is the comoving volume of the survey. The variance of  $C|_S$  is the sum of two terms:

$$\begin{aligned} \sigma_C^2 = & f_{\text{sky}}^{-1} \int dz \frac{dV^f}{dz} \int dM \frac{d\bar{n}}{dM} S^2(M, z; \lambda) \rho(\lambda|M) d\lambda \\ & + \sum_j \sigma_j^2 \left[ \int dM \frac{d\bar{n}}{dM} b(M, z_j) S(M, z_j; \lambda) \right. \\ & \quad \left. \times \rho(\lambda|M, z_j) d\lambda \Delta V_j^f \right]^2. \end{aligned} \quad (4)$$

The first term on the right hand side is often called the Poisson term. If

$$N_P \equiv \left[ \int S^2 \rho d\bar{n} dV^f d\lambda \right]^{-1} \left[ \int S \rho d\bar{n} dV^f d\lambda \right]^2 \quad (5)$$

denotes an effective number of clusters, then the fractional fluctuation in  $C_\ell$  induced by the Poisson term is  $[N_P f_{\text{sky}}]^{-1/2}$ .

The second term on the right hand side of equation (4) accounts for cluster clustering. The sum is over all redshift bins  $j$ . We choose bin sizes  $\Delta z \sim 0.1$  so that  $\delta_S$ , the mass overdensity fluctuation smoothed over the survey volume  $f_{\text{sky}} \Delta V^f$  in any given redshift bin, is (approximately) uncorrelated with  $\delta_S$  in other bins. The quantity

$$\sigma_j^2 \equiv \langle \delta_{S_j}^2 \rangle = \int P_j(k) W_j^2(\mathbf{k}) d^3k / (2\pi)^3 \quad (6)$$

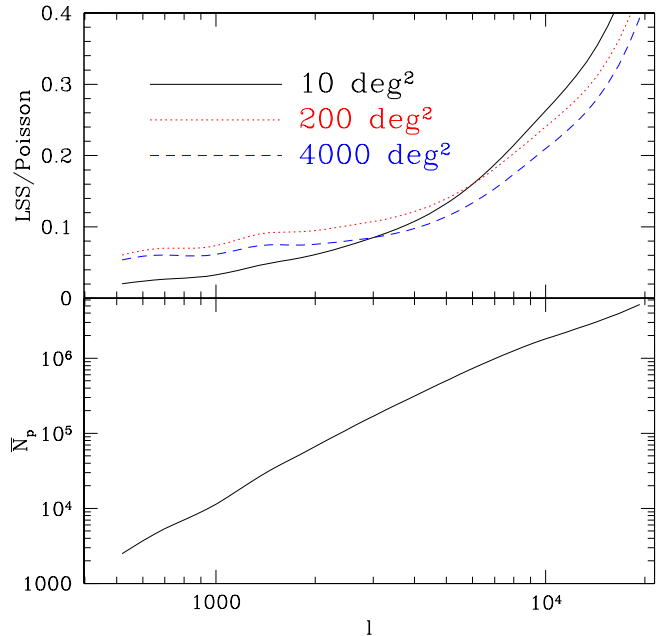


FIG. 1.— The variance of the SZ power spectrum. The lower panel shows the weighted cluster number  $\bar{N}_P$ .  $(N_P f_{\text{sky}})^{-1/2}$  is the fractional statistical error caused by the Poisson distribution of clusters. The upper panel shows the ratio between the statistical error caused by the large scale clustering and the Poisson distribution. We show below that when  $N_P f_{\text{sky}} \gg 10$ , then  $p(C_\ell)$  will approach a Gaussian form, in accordance with the central limit theorem.

is the rms of the matter over-density when smoothed over the survey window in the  $j$ th redshift bin;  $P_j$  and  $W_j$  represent the 3D matter density power spectrum, and the Fourier transform of the survey window function, both in the  $j$ th redshift bin. The factor  $b$  represents the fact that the cluster distribution is biased relative to the dark matter:  $\delta_L(M) = b(M)\delta_S$ .

We model  $S(M, z)$  using the universal gas profile of (Komatsu & Seljak 2001). This model makes three reasonable approximations/assumptions: (1) Intra-cluster gas is in hydrostatic equilibrium; (2) the gas pressure  $P_g \propto \rho_g^\gamma$  and the polytropic index  $\gamma$  is a constant; (3) the ratio of the gas density  $\rho_g$  and the dark matter density approaches the cosmological value  $\Omega_b/\Omega_{\text{DM}}$  in the outer regions of clusters. Given a dark matter profile, this model predicts  $S$  uniquely. When combined with a model for the mass function  $d\bar{n}/dM$ , this model completely specifies  $\bar{C}$  (Komatsu & Seljak 2002).

Fig. 1 shows the Poisson and halo clustering contributions to the SZ power spectrum variance for a range of choices of the fraction of sky covered  $f_{\text{sky}}$ . The top panel shows that the halo clustering contribution is subdominant, but non-negligible, at the relevant scales. Although the Poisson term has a simple dependence on the sky coverage ( $\propto f_{\text{sky}}^{-1}$ ), the halo clustering term is more complicated. It depends implicitly on  $f_{\text{sky}}$  because  $\sigma^2$  depends on the shape of the survey volume. Since the effective power index of CDM power spectrum  $n_{\text{eff}}$  varies with scale,  $\sigma^2$  has non-trivial dependence on the smoothing scale. Thus the ratio between the halo clus-

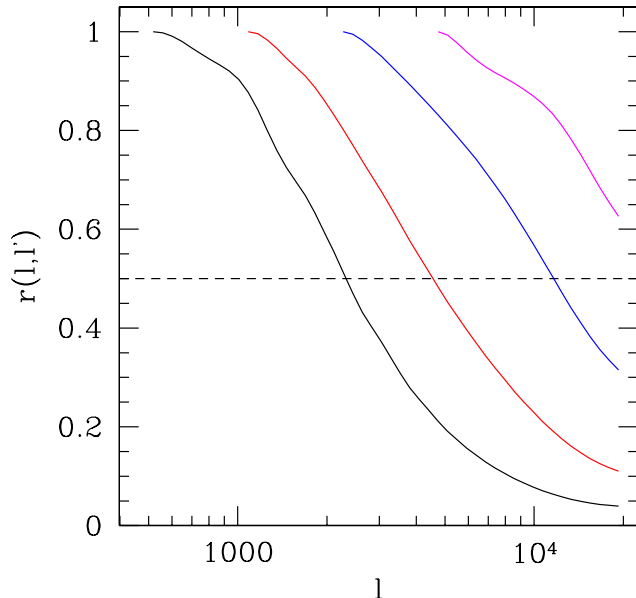


FIG. 2.— The cross correlation coefficient  $r$  between different  $\ell$  modes. The dependence of  $r$  on sky coverage is negligible; we have assumed coverage of  $200 \text{ deg}^2$ . The value of  $\ell'$  for each line is indicated by the lowest  $\ell$  value for which it is plotted.

tering term and the Poisson term has a complicated dependence on  $f_{\text{sky}}$ .

The bottom panel shows that  $N_{\text{P}}$ , the effective number of clusters, increases with increasing  $\ell$ . This reflects the fact that the small scale SZ power spectrum is dominated by smaller halos (e.g. Komatsu & Seljak (2002)). Since the Poisson contribution to the power scales as  $N_{\text{P}}^{-1/2}$ , it decreases as  $\ell$  increases. Because the bias factor also decreases with decreasing halo mass, the halo clustering contribution also decreases on small scales. However, the decrease is not as dramatic as for the Poisson term; this is why the ratio of this to the Poisson term increases with  $\ell$ .

The *universal* gas model is spherically symmetric, so different  $\ell$  with the same  $\ell \equiv |\ell|$  are identical.<sup>2</sup> Hence, the combination of  $(2\ell + 1)$  modes all having the same  $|\ell|$  has the same statistical error  $\sigma_C$  and the fractional error  $\simeq [N_{\text{P}} f_{\text{sky}}]^{-1/2}$ . For a Gaussian random field, the *fractional* statistical error of the power spectrum for each  $\ell$  is  $[(2\ell + 1) f_{\text{sky}}/2]^{-1/2}$ . Since  $N_{\text{P}} \gg \ell$  (Fig. 1), the statistical error of the SZ effect of each  $\ell$  is *smaller* than it would be in a Gaussian random field. The halo model shows that this is because clusters are nearly self similar, so the statistical error in the SZ power spectrum is mainly determined by the fluctuations in cluster number. Because there are many clusters across the sky, these fluctuations are small, and the resulting statistical error is smaller than the corresponding Gaussian estimate.

However, this does *not* mean that the statistical precision of the SZ measurement exceeds the Gaussian limit. Although clusters are nearly self similar, the contribu-

<sup>2</sup> Accounting for cluster ellipticities breaks this degeneracy as we discuss in §4.

tion of each cluster spans a large range in  $\ell$ . As a result, the observed signal in the different  $\ell$  modes can be highly correlated. If  $\Delta\ell_c$  denotes the correlation length in  $\ell$  space, then it is the combined error on  $\Delta\ell_c$  modes which is the same as that of one single mode. This can be much larger than the corresponding Gaussian error  $[(2\ell + 1) \Delta\ell_c f_{\text{sky}}/2]^{-1/2}$ .

To estimate  $\Delta\ell_c$  we compute the covariance between  $C_\ell$  and  $C_{\ell'}$ :

$$\begin{aligned} \text{Cov}_{\ell\ell'} &= f_{\text{sky}}^{-1} \int dz \frac{dV^f}{dz} \int dM \frac{d\bar{n}}{dM} S S' \rho(\lambda|M) d\lambda \\ &+ \sum_j \sigma_j^2 \left[ \int dM \frac{d\bar{n}}{dM} b S \rho(\lambda) d\lambda \Delta V_j^f \right] \\ &\times \left[ \int dM \frac{d\bar{n}}{dM} b S' \rho(\lambda) d\lambda \Delta V_j^f \right] \quad (7) \end{aligned}$$

where  $S' \equiv S_{\ell'}(M, z; \lambda)$ . Again, the Poisson term dominates this covariance. The cross correlation coefficient between the statistical errors of  $C_\ell$  and  $C_{\ell'}$  is

$$r^2 \equiv \frac{\text{Cov}_{\ell\ell'}}{\sigma_C^2 \sigma_{C'}^2}. \quad (8)$$

Since the Poisson term dominates in both the variance and covariance term, the dependence of  $r$  on  $f_{\text{sky}}$  is negligible.

Fig. 2 shows  $r$  for  $200 \text{ deg}^2$  sky coverage. Note that the correlation length  $\Delta\ell_c \gtrsim 1000$ . In simulations, the finite size of the SZ map  $\theta_{\text{map}}$ , makes the natural bin size  $\Delta\ell = 2\pi/\theta_{\text{map}} \sim 300$  for typical  $\theta_{\text{map}} \sim 1^\circ$ . Thus,  $\ell$  modes over this  $\Delta\ell$  can be treated as completely correlated. The fractional statistical error on  $C$  measured in simulations, with respect to the Gaussian random field, is expected to be  $\sim [\ell\Delta\ell/N_{\text{P}}]^{1/2}$ . This is indeed what is seen. For example, the analysis above suggests that the quantity shown in Fig.6 of Zhang, Pen & Wang (2002) is  $a_4 \simeq (2\ell + 1)\Delta\ell[1 + \text{LSS}/\text{Poisson}]/N_{\text{P}} - 2$  (if the contribution of halo clustering has been taken into account). The numbers from Fig. 1 suggest that  $a_4 \sim 50$  at  $\ell = 10^3$  and  $a_4 \sim 2$  at  $\ell = 10^4$ , consistent with the simulations Zhang, Pen & Wang (2002).

### 3. THE PDF OF THE SZ POWER SPECTRUM

The quantities  $\bar{C}$ ,  $\sigma_C$  and  $\text{Cov}_{\ell\ell'}$  are the lowest order moments of the power spectrum PDF  $p(C_\ell)$ . However, because the SZ signal is non-Gaussian, these low order moments do not uniquely determine  $p(C_\ell)$ . Since  $p(C_\ell)$  is required to make unbiased error analyses and parameter constraints, this section provides an analytical integral formula for  $p(C_\ell)$ . This integral form, which is based on the halo model, allows fast numerical calculation and has the flexibility to incorporate much of the relevant physics. For clarity, § 3.1 considers the case of a single redshift bin; the contributions from different bins are summed in § 3.2.

#### 3.1. Single redshift bin

Given a survey and a redshift bin, the survey volume is fixed. We sort the clusters in this volume into bins of  $M$  and, in principle, bins in the other parameters  $\lambda_i$ . Then the overall SZ power spectrum is

$$C = f_{\text{sky}}^{-1} \sum_{\alpha} N_{\alpha} S_{\alpha}, \quad (9)$$

where  $N_\alpha$  is the number of clusters in the  $\alpha$ -th bin and  $S_\alpha$  is the SZ power spectrum of each cluster in the  $\alpha$ -th mass (and  $\lambda$ ) bin. The PDF of  $C$  in the  $j$ th redshift bin is

$$p_j(C) = \sum_{N_1=0}^{\infty} \cdots \sum_{N_\alpha=0}^{\infty} P(N_1, \dots, N_\alpha) \quad (10)$$

$$\times \delta_D \left( f_{\text{sky}}^{-1} \sum_{\alpha} N_\alpha S_\alpha - C \right), \quad (11)$$

where  $P(N_1, \dots, N_\alpha)$  is the joint distribution of the  $N_\alpha$ .

This distribution is computed in two steps. First, if the matter overdensity  $\delta$  in the survey volume is not exactly zero, then the mean number of expected clusters is altered (Mo & White 1996; Sheth & Tormen 2002). We use

$$N_{\alpha,L} = \bar{N}_\alpha (1 + \delta_\alpha) \quad (12)$$

to denote this altered mean. We then convert the smooth field  $N_{\alpha,L}$  to a discrete point process by assuming a Poisson sampling model. Namely, we assume that given  $\delta_\alpha$ ,

$$P_P(N_\alpha | \delta_\alpha) = \frac{[N_{\alpha,L}]^{N_\alpha}}{N_\alpha!} \exp[-N_{\alpha,L}]; \quad (13)$$

note that this Poisson process in the  $\alpha$ th bin is independent of that in the other bins. Hence,

$$P(N_1, \dots, N_\alpha) = \int \left[ \prod_{\alpha} P_P(N_\alpha | \delta_\alpha) \right] \times P_L(\delta_1, \dots, \delta_\alpha) \prod_{\alpha} d\delta_\alpha. \quad (14)$$

To proceed, we need a model for  $P_L(\delta_1, \dots, \delta_\alpha)$ , the joint PDF of  $\delta_\alpha$ .

When the volume is small, stochastic discreteness effects dominate, and  $P_L(\delta_1, \dots, \delta_\alpha) \rightarrow \prod_{\alpha} P_L(\delta_\alpha)$ . When this limit applies, the Poisson fluctuation is much larger than the matter fluctuation and the exact form of  $P_L$  is not necessary. However,  $P_L(\delta_1, \dots, \delta_\alpha)$  in the general case is more complicated (Sheth & Lemson 1999).

When  $\delta_\alpha \ll 1$ , then the linear bias model

$$\delta_\alpha = b_\alpha \delta \quad (15)$$

works well (Mo & White 1996; Sheth & Tormen 2002), and

$$P_L \rightarrow P_\delta \prod_{\alpha} \delta_D(\delta_\alpha - b_\alpha \delta). \quad (16)$$

Typically, this requires the volume to be larger than about  $(100h^{-1}\text{Mpc})^3$ . In practice we will apply the linear bias model to all relevant cases.

To see what linear bias implies, note that the characteristic function is

$$\begin{aligned} \tilde{p}_j &\equiv \int dC p_j(C) \exp(i\tilde{f}C) \quad (17) \\ &= \int P_L(\delta_1, \dots, \delta_\alpha) \prod_{\alpha} d\delta_\alpha \\ &\quad \times \exp \left[ \sum_{\alpha} N_{\alpha,L} (e^{i\tilde{f}S_\alpha} - 1) \right], \\ &= \int d\delta P_j(\delta) \exp \left\{ \int [\exp(i\tilde{f}S(\lambda)) - 1] dN_L \right\} \end{aligned}$$

where  $\tilde{f} \equiv f/f_{\text{sky}}$ . The second equality uses the Poisson model, and the final expression uses the linear bias model in the limit that the mass (and  $\lambda$ ) bin size goes to zero. I.e.,  $dN_L = d\bar{N}(1+b\delta)$  is the expected number of clusters in the survey volume and redshift and mass bin (without Poisson fluctuation), and  $d\bar{N}/f_{\text{sky}}$  is the expected number of clusters averaged over the whole sky. Our notation makes explicit that the distribution  $P_j(\delta)$  of the mass density fluctuations  $\delta$  may depend on redshift.

On large scales, the distribution of  $\delta$  should be approximately Gaussian:  $P_j(\delta) \propto \exp(-\delta^2/2\sigma_j^2)$ . Hence, for each redshift bin,

$$\tilde{p}_j = \exp \left( f_{\text{sky}} D_j + \frac{f_{\text{sky}}^2 E_j^2 \sigma_j^2}{2} \right), \quad (18)$$

where

$$D_j = f_{\text{sky}}^{-1} \int d\bar{N} (e^{i\tilde{f}S} - 1), \quad (19)$$

and

$$E_j = f_{\text{sky}}^{-1} \int d\bar{N} b (e^{i\tilde{f}S} - 1). \quad (20)$$

Notice that neither  $D_j$  nor  $E_j$  have any dependence on  $f_{\text{sky}}$ , because the implicit dependence of  $\bar{N}$  on  $f_{\text{sky}}$  ( $\bar{N} \propto f_{\text{sky}}$ ) cancels the  $f_{\text{sky}}^{-1}$  factor in the definitions of  $D_j$  and  $E_j$ . We will soon show that  $D_j$  describes the discreteness of the cluster distribution and  $E_j$  describes the clustering effect.

Strictly speaking, equation (18) follows from integrating the Gaussian from  $-\infty$  to  $+\infty$ . Since  $b\delta < -1$  is problematic (one may not have a negative number for the mean halo count in a cell), one might have thought the range of integration should be restricted to  $\delta \geq -1/b$ . In practice, when the survey area is large, then  $\sigma_j \ll 1$ , so  $\delta \ll 1$  and  $b\delta > -1$  almost surely, and ignoring the restriction on  $\delta$  is reasonable. This approximation simplifies the calculation in the next subsection significantly.

Before moving on, suppose that  $S$  was the same constant for all clusters. In this case,

$$\begin{aligned} f_{\text{sky}} D_j &\rightarrow (S-1) \int d\bar{N} \equiv (S-1) \bar{N}_{\text{eff}} \\ f_{\text{sky}} E_j &\rightarrow (S-1) \int d\bar{N} b \equiv (S-1) \bar{N}_{\text{eff}} b_{\text{eff}}, \quad (21) \end{aligned}$$

where we have defined  $S \equiv e^{i\tilde{f}S}$ . Hence,

$$\tilde{p}_j \rightarrow \exp \left[ (S-1) \bar{N}_{\text{eff}} + \frac{(S-1)^2}{2} \bar{N}_{\text{eff}}^2 b_{\text{eff}}^2 \sigma_j^2 \right]; \quad (22)$$

this expression is essentially the generating function of unweighted counts in cells. Notice that it agrees with the expressions derived by Hu & Cohn (2006) and Holder (2006) (although Hu & Cohn set the lower limit of the integral over  $\delta$  to  $-1/b$ ). In this respect, our analysis generalizes their work to the case in which clusters contribute different weights.

In the counts in cells case, suppose that each cluster is weighted by the number of galaxies it contains, and that  $W(S)$  is the generating function of galaxy counts per cluster. Then the generating function of galaxy counts in cells, say  $g(S)$ , is given by  $g(S) = G(W(S))$ , where  $G(S)$  is the generating function of unweighted cluster counts

(e.g. our Eq. 22). We have used  $W(S)$  to emphasize that one can think of the galaxy counts in cells distribution as arising from a process where each cluster is weighted differently (i.e., by the number of galaxies in it).

In our SZ calculation, each cluster has a different weight, so we can think of  $W(S)$  as having a different value for each cluster. So our Eq. 17 is indeed equivalent to the counts in cells analogy. This analogy also shows how to generalize our formalism to include scatter in halo concentrations  $\rightarrow$  scatter in SZ signal,  $\rightarrow$  scatter in SZ  $C_\ell$  even at fixed halo mass.

One might have thought that equation (18) fails in the limit of small sky coverage. Appendix A shows that, in fact, it agrees with the Poisson (small sky coverage) limit to order  $\sigma^2$ . This agreement gives us the confidence to apply equation (18) to any relevant survey area.

### 3.2. Projection along the line of sight

The SZ power spectrum is obtained by summing over all redshift bins. Since the contributions from different redshift bins are correlated, the relation between the PDF of the total SZ power spectrum and the PDF of the SZ power spectrum from each redshift bin is complicated. However, for a sufficiently wide bin in  $z$ , e.g.  $\Delta z = 0.1$ , the fluctuations  $\delta_z$  of different redshift bins are approximately uncorrelated. In this case, the Fourier transform of the SZ power spectrum PDF is just the product of equation (18) for each redshift bin,

$$\begin{aligned} \tilde{P} &= \prod_j \tilde{p}_j = \exp \left[ \sum_j \left( D_j f_{\text{sky}} + \frac{E_j^2 \sigma_j^2 f_{\text{sky}}^2}{2} \right) \right] \\ &\equiv \exp \left[ G(\tilde{f}) \right]. \end{aligned} \quad (23)$$

Here,  $j$  denotes the  $j$ -th redshift bin.

The Inverse Fourier transform of equation (23) yields the PDF

$$P(C_\ell) = \int \tilde{P} \exp(-ifC_\ell) df / (2\pi). \quad (24)$$

Equation (23) has all desired quantities: (1)  $\tilde{P}^*(f) = \tilde{P}(-f)$ , so the PDF is real; (2)  $\tilde{P}(f=0) = 1$ , so  $\int P(C) dC = 1$ , meaning the PDF is correctly normalized. It is straightforward to verify that  $d\tilde{P}/df|_{f=0} = i\bar{C}$  and  $d^2\tilde{P}/df^2 = -(\bar{C}^2 + \sigma_C^2)$  reduce to the expressions for  $\bar{C}$  and  $\sigma_C^2$  given in the previous section (equations 3 and 4 respectively). This shows explicitly that our expression for  $P(C)$  has the correct first and second moments.

### 3.3. 2-point joint pdf of $C_\ell$ and $C_{\ell'}$

The joint pdf of  $P_2(C_\ell, C_{\ell'})$  can be derived similarly. The 2D Fourier transform is

$$\tilde{P}_2(f, f') \equiv \int \int P_2(C, C') \exp(iff + if' C') df df'. \quad (25)$$

For a single redshift,

$$\begin{aligned} \tilde{P}_2 &= \int P_L(\delta_1, \dots, \delta_\alpha) \prod_\alpha d\delta_\alpha \\ &\times \exp \left[ \sum_\alpha N_{\alpha,L} \left( e^{ifS_\alpha + if' S'_\alpha} - 1 \right) \right]. \end{aligned} \quad (26)$$

Again, assuming the linear bias model and Gaussian  $p_j(\delta)$  yields

$$\ln \tilde{P}_2 = \sum_j f_{\text{sky}} D_{2j} + \frac{f_{\text{sky}}^2 E_{2j}^2 \sigma_j^2}{2} \equiv G_2(\tilde{f}, \tilde{f}'), \quad (27)$$

where

$$D_2 = f_{\text{sky}}^{-1} \int d\bar{N} \left[ e^{ifS + if' S'} - 1 \right], \quad (28)$$

and

$$E_2 = f_{\text{sky}}^{-1} \int d\bar{N} b \left[ e^{ifS + if' S'} - 1 \right]. \quad (29)$$

It is straightforward to verify that this expression is normalized to unity, and that the expressions for  $\bar{C}, \bar{C}', \sigma_C, \sigma_{C'}$  and  $\text{Cov}_{\ell\ell'}$  which it implies are all in agreement with our previous expressions (e.g. equation 7).

If  $G_2(\tilde{f}, \tilde{f}')$  can be written as the sum of two terms, one a function of  $\tilde{f}$  and the other of  $\tilde{f}'$ , then this would imply that  $C$  and  $C'$  are independent. The expression above shows that, in general, this condition is not satisfied. For example, there are cross terms in both  $D$  and  $E^2$  which imply correlations between  $C$  and  $C'$ . In the limit that  $\ell$  and  $\ell'$  are sufficiently different that  $S \gg S'$  (or  $S \ll S'$ ), then  $D_2$  roughly meets this condition. Since the correlation induced by the  $E_2^2$  term is weak, the resulting  $P_2(C, C') \simeq P(C)P(C')$ .

### 3.4. $n$ -point joint pdf of $C_\ell$ and $C_{\ell'}$

The analysis above for the Fourier Transform of the 2-point pdf is easily generalized to that for the  $n$ -point pdf:

$$\begin{aligned} \ln \tilde{P}_n(f_1, \dots, f_n) &\equiv \ln \int \int P_n(C_1, \dots, C_n) \\ &\times e^{if_1 C_1 + \dots + if_n C_n} df_1 \dots df_n \\ &= \sum_j f_{\text{sky}} D_{nj} + \frac{f_{\text{sky}}^2 E_{nj}^2 \sigma_j^2}{2}, \end{aligned} \quad (30)$$

where

$$D_n = f_{\text{sky}}^{-1} \int d\bar{N} \left[ e^{if_1 S_1 + \dots + if_n S_n} - 1 \right], \quad (31)$$

and

$$E_n = f_{\text{sky}}^{-1} \int d\bar{N} b \left[ e^{if_1 S_1 + \dots + if_n S_n} - 1 \right]. \quad (32)$$

Equation (30) for the  $n$ -point PDF and its special cases, equations (23) and (27) for the 1- and 2-point PDFs, are the key results of this paper.

### 3.5. The large sky coverage limit

To better understand the physical meaning of the terms in equations (23), (27) and (30), it is useful to study the limit of large sky coverage.

Consider the one point pdf  $P(C)$  in this limit. Effectively, only those modes with  $\text{Re}[G(\tilde{f})] \gtrsim -10$  contribute to  $P$ . Over this range of  $\tilde{f}$ ,  $\text{Re}[G]$  decreases with  $\tilde{f}$ . Thus, those modes with  $\text{Re}[G] \gtrsim -10$  have

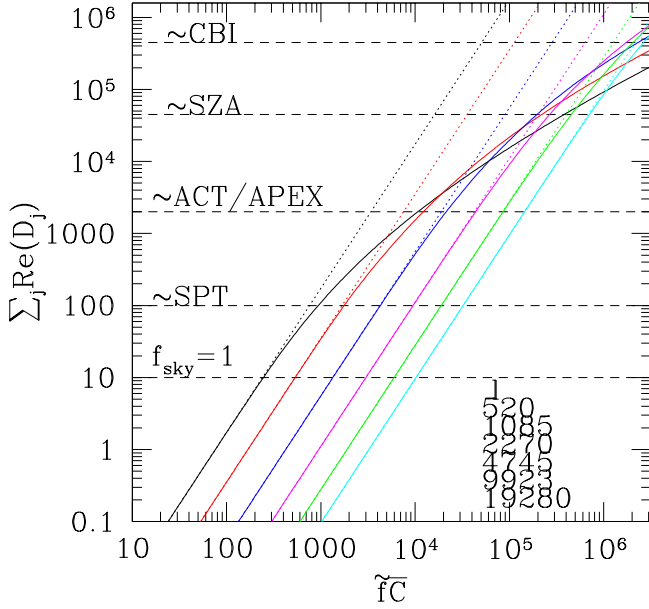


FIG. 3.— The requirement for having a Gaussian PDF. Solid lines show  $\text{Re}(\sum_j D_j)$  for several multipoles. Straight dotted lines are  $\propto f^2$ . The deviation of the dotted lines from the corresponding  $f$  modes implies that the pdf is non-Gaussian. The  $\tilde{f}$  modes below the straight dashed lines are the relevant modes for corresponding sky coverage (SPT:  $\sim 4000 \text{ deg}^2$ ; ACT/APEX:  $\sim 200 \text{ deg}^2$ ; SZA:  $\sim 10 \text{ deg}^2$  and CBI:  $\sim 1 \text{ deg}^2$ ).

$\tilde{f} \lesssim \tilde{f}_c$ , where  $\text{Re}[G(\tilde{f}_c)] = -10$ . Since  $|\text{Re}(G)|$  increases with  $f_{\text{sky}}$ ,  $\tilde{f}_c$  decreases with  $f_{\text{sky}}$ . Thus, for sufficiently large  $f_{\text{sky}}$ ,  $\tilde{f}_c$  and so all relevant  $\tilde{f}$  are small, and  $\exp(i\tilde{f}C) - 1 \simeq i\tilde{f}C - (\tilde{f}C)^2/2$ . In this case,

$$\text{Im}(D_j) \simeq \tilde{f}\bar{C}_j, \quad \text{Re}(D_j) \simeq -\frac{\tilde{f}^2 \bar{C}_j^2}{2 \bar{N}_j},$$

$$\text{Im}(E_j) \simeq \tilde{f}\bar{b}_j\bar{C}_j, \quad \text{Re}(E_j) \simeq 0, \quad \text{and} \quad (33)$$

$$\begin{aligned} G(\tilde{f}) &\simeq i\tilde{f}\bar{C} - \frac{f^2}{2} \sum_j \bar{C}_j^2 \left[ \frac{1}{N_{\text{P}j} f_{\text{sky}}} + \bar{b}_j^2 \sigma_j^2 \right] \\ &= i\tilde{f}\bar{C} - \frac{f^2 \sigma_C^2}{2}. \end{aligned} \quad (34)$$

Here,

$$\begin{aligned} \bar{C}_j &\equiv f_{\text{sky}}^{-1} \int S(\lambda) d\bar{N}_j, \quad N_{\text{P}j} \equiv f_{\text{sky}}^{-1} \frac{[\int S(\lambda) d\bar{N}_j]^2}{\int S(\lambda)^2 d\bar{N}_j} \quad \text{and} \\ \bar{b}_j &\equiv \frac{\int S(\lambda) b(\lambda) d\bar{N}_j}{\int S(\lambda) d\bar{N}_j} \end{aligned} \quad (35)$$

are all defined in the  $j$ -th redshift bin.  $\bar{C}$  is defined by equation (3) and  $\bar{C} = \sum \bar{C}_j$ . None of these quantities depends on  $f_{\text{sky}}$ . Notice that the coefficient of  $f^2/2$  in equation (34) is just the variance of  $C$  (equation 4). Thus, in the large sky limit, there are sufficiently many clusters that the Poisson distribution becomes Gaussian, in accordance with the central limit theorem. Thus  $P$ , the Fourier transform of  $\exp[G]$ , will also be Gaussian.

When the above conditions are satisfied, the Fourier transforms of equations (23) and (34) yield

$$P(C) = \frac{1}{\sqrt{2\pi}\sigma_C} \exp\left(-\frac{(C - \bar{C})^2}{2\sigma_C^2}\right), \quad (36)$$

where  $\bar{C}$  and  $\sigma_C$  are given by equations (3) and (4), respectively. This shows that, in the limit of large sky coverage,  $P(C)$  becomes Gaussian.

However, the conditions (33) are not always satisfied. The condition  $\text{Re}(D_j) \simeq (f/f_{\text{sky}})^2 \bar{C}_j^2 / \bar{N}_j$  is especially hard to meet. Since the term  $\text{Re}(\sum_j D_j)$  dominates that involving  $\sum_j E_j^2$  (consistent with Fig. 1), requiring that

$$\sum_j \text{Re}(D_j) \propto f^2 \quad \text{when} \quad f_{\text{sky}} \sum_j \text{Re}(D_j) \geq -10, \quad (37)$$

is a suitable condition for Gaussianity. We call this the *Gaussian condition*. Fig. 3 shows that, for an all sky survey, all  $\ell > 500$  satisfy the Gaussian condition given above. For SPT, the Gaussian condition is satisfied at  $\ell \gtrsim 10^3$ . However, for small sky coverage survey such as SZA, the Gaussian condition is only satisfied at  $\ell \gtrsim 10^4$ .

In the limit of large sky coverage, one can Taylor expand  $G_2$  around  $\tilde{f}, \tilde{f}' = 0$ , keeping terms up to  $\tilde{f}^2, \tilde{f}'^2$ . The resulting 2-point joint PDF takes the Gaussian form

$$P_2 \propto \exp\left[-\frac{X^2 + X'^2 - 2XX'r}{2(1-r^2)}\right], \quad \text{where} \quad X = \frac{C - \bar{C}}{\sigma_C} \quad (38)$$

and  $r$  is given by equation (8). If  $\ell' \sim \ell$ , then  $C_\ell$  and  $C_{\ell'}$  are dominated by contributions from halos with similar  $M, z$  and  $\lambda_\ell$ . So we expect  $C_\ell$  and  $C_{\ell'}$  to be highly correlated. Their correlation is quantified by  $r$  and as expected, when  $\ell' \rightarrow \ell, r \rightarrow 1$ . When  $\ell'$  differs significantly from  $\ell$ ,  $C_\ell$  and  $C_{\ell'}$  are dominated by different clusters, so  $r \rightarrow 0$ , meaning  $C_\ell$  and  $C_{\ell'}$  are nearly independent.

### 3.6. Numerical evaluation of the PDF

The integral form of the  $n$ -point SZ power spectrum PDF (equation 30) must be computed numerically. This is straightforward for the 1- and 2-point pdfs, but more sophisticated Monte-Carlo methods must be used for efficient evaluation when  $n$  is large. In what follows, we illustrate our results using the 1-point pdf (equation 23).

The solid curves in Figs. 4, 5 and 6 show equation (23) for surveys covering 1, 10, 200 and 4000  $\text{deg}^2$ . For comparison, we also show the corresponding Gaussian form (equation 36). For 1  $\text{deg}^2$  sky coverage, representative of CBI,  $P(C)$  is highly non-Gaussian at  $\ell \lesssim 4000$ . This is consistent with what would be expected from Fig. 3, which shows that a significant fraction of the relevant modes deviate from the  $\text{Re}\sum D_j \propto f^2$  scaling, so the Gaussian condition (equation 37) is not satisfied. Further understanding of this non-Gaussian behavior comes from Fig. 1: the effective number of clusters contributing to the SZ effect is  $N_{\text{P}} f_{\text{sky}} \lesssim 10$  for  $\ell < 4000$ . So we expect large Poisson fluctuations in the SZ power spectrum for  $\ell < 4000$ . Although  $N_{\text{P}}$  increases with  $\ell$ , making the non-Gaussianity weaker at higher  $\ell$ , it is still only  $\sim 30$  at  $\ell = 10^4$ , so we expect  $P(C)$  to be mildly non-Gaussian even at  $\ell = 10^4$ . For 10  $\text{deg}^2$  sky coverage, roughly the area SZA<sup>3</sup> plans to cover,  $P(C)$  is strongly skewed at

<sup>3</sup> SZA, <http://astro.uchicago.edu/sza/>

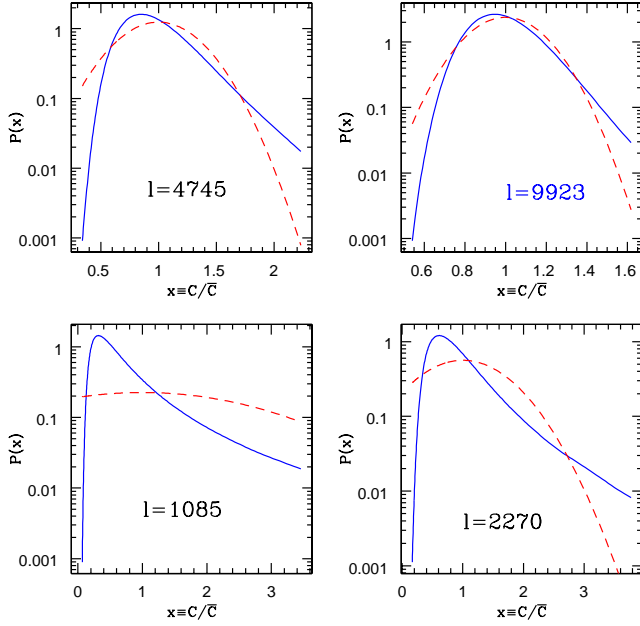


FIG. 4.— The PDF of  $C \equiv C_\ell$  for  $\ell = 1085, 2270, 4745, 9923$ , respectively in a  $1 \text{ deg}^2$  survey. Solid lines show the pdf given by equation (23), and dashed lines show a Gaussian form with the same mean  $\bar{C}$  and  $\sigma_C$  for comparison.  $P(C)$  is highly non-Gaussian for  $\ell \lesssim 4000$ , mainly because the small survey volume means that discreteness fluctuations in the cluster counts are large (c.f. Fig. 3).

$l \lesssim 2000$ , with a non-negligible tail at high  $C$ . Only for multipoles  $\gtrsim 5000$ , where  $N_p f_{\text{sky}} \gtrsim 100$  (Fig. 1), does  $P(C)$  approach the Gaussian form (Fig. 5). For larger sky coverage,  $P(C)$  becomes more Gaussian. For a  $200 \text{ deg}^2$  survey, roughly ACT<sup>4</sup> and APEX<sup>5</sup> plans to cover,  $P(C)$  approaches Gaussian at  $l \gtrsim 2000$ . Note, however, analysis of the SZ power spectrum at  $l \lesssim 2000$  must account for the fact that the pdf is non-Gaussian. Again, these results are consistent with expectations based on Figs. 1 and 3.

For  $4000 \text{ deg}^2$  sky coverage, roughly the size of SPT<sup>6</sup>,  $P(C)$  is Gaussian at  $l \gtrsim 1000$ . For Planck, which will cover the full sky,  $P(C)$  can be assumed to be Gaussian distributed at all relevant scales. While this will significantly simplify the analysis of the SPT and Planck SZ power spectra, we caution that the variance of this Gaussian differs significantly from that expected in a truly Gaussian random field (fig. 1). The strong correlation between different  $\ell$  modes makes the total S/N of the SZ power spectrum significantly smaller than that of a random Gaussian field.

In our model, the SZ power spectrum is dominated by contributions from single halos (the one-halo term), and we have attributed the non-Gaussianity in the SZ  $p(C_\ell)$  we find to Poisson fluctuations in the halo number distribution. In this model, different  $l$  modes of the SZ effect can be highly correlated, with correlation length  $\Delta\ell_c$  comparable to  $\ell$  (Fig. 2). Hence, the PDF of the

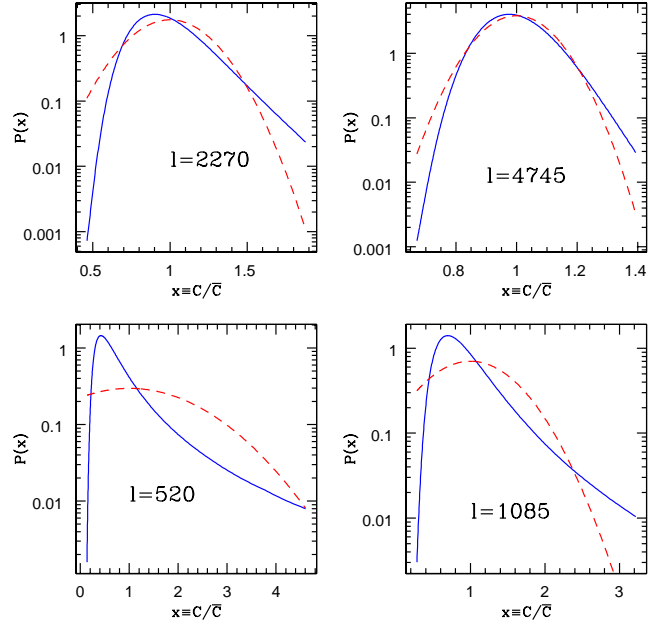


FIG. 5.— Similar to Fig. 4, but for  $10 \text{ deg}^2$  sky coverage and  $\ell = 520, 1085, 2270, 4745$ , respectively. The non-Gaussianity is weaker compared to that in Fig. 4, because the larger number of clusters in the survey volume brings the Poisson fluctuations closer to the Gaussian limit.

band power with width  $\Delta\ell$  is roughly the same as the PDF of a single mode, as long as  $\Delta\ell \leq \Delta\ell_c$ . The strength of the non-Gaussianity in this band power PDF is then also determined by the effective number of halos in the survey volume, which is  $N_p f_{\text{sky}}$ .

However, there is another possible origin of the non-Gaussian PDF. Suppose that the distribution of SZ temperature fluctuations were exactly Gaussian. Then  $p(C_\ell)$  would follow a  $\chi^2$ -distribution, so one might wonder if this is the origin of the non-Gaussianity seen in Figs. 4, 5 and 6? The argument for band-powers, rather than single modes, is similar: If  $Y_i$  is the  $i$ -th Fourier mode, and we define the normalized band power  $x = \sum_i^n |Y_i|^2 / (n\bar{C})$ , where  $\bar{C}$  is the mean variance of the  $Y_i$ , then  $x$  is the average of  $n$  independent Fourier modes. If we approximate the variance in each mode as being the same as  $\bar{C}$ , then

$$P_n(x) = \frac{2^{-n}}{\Gamma(n)} x^{n-1} \exp(-x/2) 2n. \quad (39)$$

is a  $\chi^2$ -distribution with  $2n$  degrees of freedom (recall each  $Y_i$  has independent real *and* imaginary parts). Note that  $P_n(x)$  becomes increasingly Gaussian in shape as  $n \gg 1$ , but it is very non-Gaussian for small  $n$ .

For a survey with fractional sky coverage  $f_{\text{sky}}$ ,  $n = \ell\Delta\ell f_{\text{sky}}$ , where setting the bin size  $\Delta\ell$  equal to the correlation scale  $\Delta\ell_c$  is a natural choice. Hence, if  $n = \ell\Delta\ell_c f_{\text{sky}} \gg N_p f_{\text{sky}}$ , then the non-Gaussianity in the band power PDF will be mainly contributed by Poisson fluctuations in halo number. Now, Fig. 2 shows that  $\Delta\ell_c \sim \ell$ , and Fig. 1 shows that, at  $\ell \sim 10^3$ ,  $N_p \approx (\ell/10)^2$ , so  $n \approx \ell^2$  is indeed larger than  $N_p \approx (\ell/10)^2$ . This shows that the non-Gaussian shape of  $p(C_\ell)$  in our model is dominated by the Poisson fluctuations in halo

<sup>4</sup> ACT, <http://www.physics.princeton.edu/act/>

<sup>5</sup> APEX, <http://bolo.berkeley.edu/apexsz/index.html>

<sup>6</sup> SPT, <http://spt.uchicago.edu/>



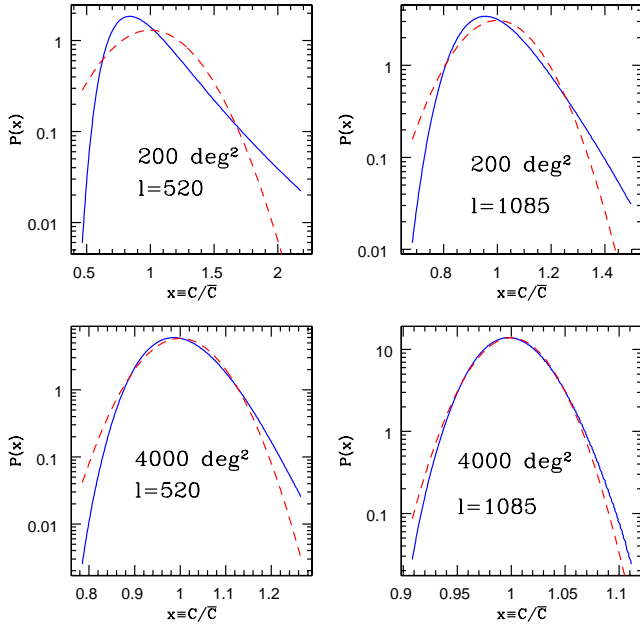


FIG. 6.— Similar to Fig. 5, but for 200 and 4000  $\text{deg}^2$  sky coverage and  $\ell = 520, 1085$ , respectively. Comparison with the smaller surveys shown previously (1 and 10  $\text{deg}^2$ ) shows that the pdf becomes increasing Gaussian as the sky coverage increases.

(cluster) counts; Fig. 7 shows this explicitly.

The PDF of the SZ power spectrum is similar to that expected from gravitational lensing in several respects: (1)  $P(C)$  is skewed so that it peaks at  $C < \bar{C}$ ; (2) It has a long tail extending to high  $C$ . For BIMA/CBI, this increases the probability of having  $C \geq 2\bar{C}$  at the relevant  $\ell$  range. When combined with the large sample variance caused by strong correlations between different  $\ell$  modes, this may help reduce the tension between the CBI/BIMA power excess relative to the naive expectations based on primary CMB and the Gaussian model of  $P(C)$ . We postpone a quantitative discussion of this issue to elsewhere.

However, the angular scale dependence of the SZ power spectrum PDF is distinctively different from that due to gravitational lensing. The lensing  $C_\ell$  is dominated by the two-halo term at large scales, whereas the SZ power spectrum is always dominated by the one-halo term (Komatsu & Kitayama 1999). Hence the pdf induced by lensing is expected to become Gaussian at large angular scales (small  $\ell$ ), whereas the SZ PDF becomes Gaussian at small angular scales (large  $\ell$ ) (Zhang & Pen (2001) and see Figs. 4, 5, and 6). Furthermore, the large scale SZ power is mainly contributed by massive clusters, whose number density is low (e.g. Komatsu & Seljak (2002) and Fig. 1). This causes large Poisson fluctuations and strong deviation from Gaussianity at large scales. On smaller scales, where more and more small clusters contribute, the Poisson fluctuations tend to the Gaussian limit.

A remaining question is the dependence of  $p(C_\ell)$  on cosmological parameters, especially  $\sigma_8$ . A convenient measure of  $p(C_\ell)$  is the effective number of clusters  $N_P$  (equation 5). There are essentially two effects: (1) A

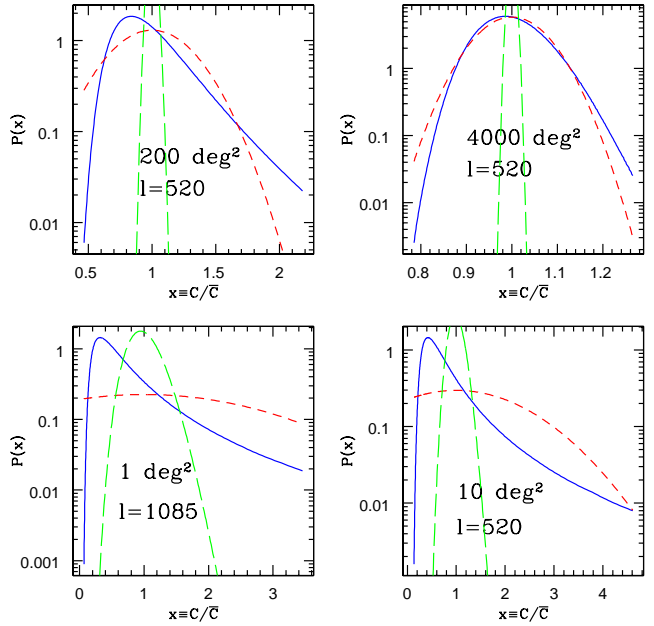


FIG. 7.— The origin of the non-Gaussianity in the SZ band power spectrum PDF. If the SZ signal were Gaussian distributed, then the PDF of the SZ band-power would follow a  $\chi^2$ -distribution with  $2\ell\Delta\ell f_{\text{sky}}$  degrees of freedom, and one might wonder if this was the origin of the non-Gaussian shape of the SZ PDF. To illustrate that this is not the origin of the non-Gaussianity in our model, the long-dashed lines show Chi-square distributions when  $(\ell, \Delta\ell) = (520, 400)$  and  $(1085, 800)$ , respectively. They are clearly different from the solid curves which show the PDF predicted by our model; short dash lines show a Gaussian form with the same rms. (In fact, because close  $\ell$  modes are strongly correlated, the true PDF of the SZ band power with bin size  $\Delta\ell \leq \Delta\ell_c$  is roughly the same as the PDF of a single Fourier mode (Fig. 4, 5 and 6), so we have simply copied the corresponding curves here.)

change in  $\sigma_8$  changes the concentrations of halos, and hence relative weights of clusters. Since  $N_P$  is the number of clusters weighted by their SZ contributions, change in  $c$  affects  $N_P$ . (i) Roughly, a cluster contributes to the SZ power spectrum only at scales larger than  $r_s = r_{\text{vir}}/c \propto M^{1/3}/c$ ; the SZ signal from a cluster is smooth on scales smaller than  $r_s$ . Here,  $c$  is the concentration parameter and  $r_{\text{vir}}$  is the virial radius of a cluster of mass  $M$ . Since  $c$  decreases with increasing mass, massive clusters only contribute to the SZ signal on relatively large scales; whereas lower mass clusters contribute down to smaller scales. Now, increasing  $\sigma_8$  makes clusters of a fixed mass more concentrated—at fixed mass  $r_s$  decreases. Thus, a massive cluster which does not contribute power to a given scale if  $\sigma_8$  is low may be able to contribute at higher  $\sigma_8$ . Thus, increasing  $\sigma_8$  increases the contribution from rarer more massive clusters. (ii) Increasing  $\sigma_8$  is expected to increase  $c$  by the same fraction for all masses (Bullock et al. 2001; Wechsler et al. 2002; Zhao et al. 2003). However, a constant fractional increase in  $c$  results in larger fractional increase in the SZ flux from a more massive cluster. Thus the weighting of more massive clusters in the SZ power spectrum is increased when increasing  $\sigma_8$ . (2) Increasing  $\sigma_8$  increases the number density of massive clusters, making  $N_P$  larger and so Poisson fluctuations in cluster abun-

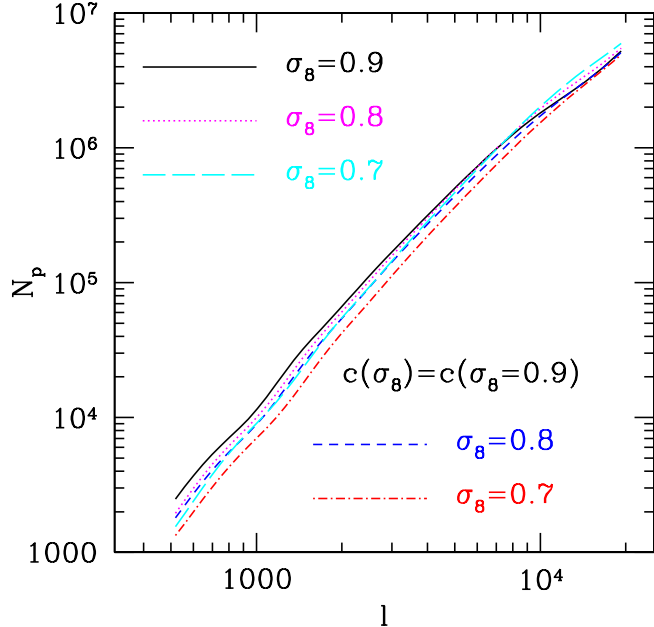


FIG. 8.— Dependence of the effective number of clusters  $N_P$  (equation 5) on  $\sigma_8$ . The short-dashed ( $\sigma_8 = 0.8$ ) and dot-dashed lines ( $\sigma_8 = 0.7$ ) have the same relation between concentration  $c$  and halo mass  $m$  as when  $\sigma_8 = 0.9$ . Hence, the difference in  $N_P$  is entirely due to the change in the mass function  $dn/dm$ . At large  $l$ , where less massive clusters dominate, the dependence on  $\sigma_8$  is negligible. This is because the abundance of the most massive clusters is exponentially sensitive to  $\sigma_8$ , whereas less massive clusters are less strongly dependent on  $\sigma_8$ . The dotted ( $\sigma_8 = 0.8$ ) and long-dashed ( $\sigma_8 = 0.7$ ) lines account for the additional fact that halo concentrations also depend on  $\sigma_8$ . This dependence partly cancels that from  $dn/dm$ . At small  $l$ , the effect on  $dn/dm$  dominates; at large  $l$ , the effect on  $c$  dominates. Hence, at  $l \sim 10^4$ ,  $N_P$  when  $\sigma_8 = 0.7$  is larger than when  $\sigma_8 = 0.9$ .

dances smaller.

Effect (1) means that increasing  $\sigma_8$  increases the relative contribution of the rarer more massive clusters (by increasing  $c$ ); if cluster abundances were not also altered, this would decrease  $N_P$  (since massive clusters are rarer). However, increasing  $\sigma_8$  also increases the number of more massive clusters (effect 2), so the two effects act in approximately opposite directions. Figure 8 shows the result of an explicit calculation of how  $N_P$  depends on  $\sigma_8$ : the two effects do indeed approximately cancel.

When expressed as a function of  $x \equiv C_\ell/\bar{C}_\ell$ , the PDF  $p(C_\ell)$  is approximately invariant to changes in  $\sigma_8$ . This provides some analytic support for the procedure of Dawson et al. (2006) which we discussed in the Introduction. However, our analysis indicates that this procedure is only approximately correct. In reality, effects (1) and (2) do not cancel exactly; we do see differences in  $N_P$  and  $p(C_\ell)$  as  $\sigma_8$  is varied. Robust evaluation of the net effect requires improvements to the models we use for cluster abundance, the  $c - M$  relation and the gas model, as well as the incorporation of several complexities which we discuss in the next section. These improvements will be addressed elsewhere.

#### 4. SUMMARY, DISCUSSION OF LIMITATIONS, AND EXTENSIONS

We have derived an analytic estimate of the  $n$ -point PDF of the SZ power spectrum (equation 30). Our derivation is based on the halo-model. The analytical integral form of the PDF allows fast calculation of the one- and two-point pdfs,  $P(C_\ell)$  and  $P(C_\ell, C_{\ell'})$  (equations 23 and 27). More advanced integration routines are required to compute higher-order PDFs in reasonable timeframes.

We find that the non-Gaussianity of the SZ power spectrum is a function of scale  $l$ , and, at fixed  $l$ , is a strong function of the survey area (Figs. 4, 5 and 6). This strong non-Gaussianity may resolve the discrepancy between CBI/BIMA SZ measurements and the primary CMB measurements. For survey areas  $\sim 10 \text{ deg}^2$ , which will be achieved by ongoing surveys such as SZA, the non-Gaussianity is significant at  $l \lesssim 4000$ , but becomes negligible at  $l \gtrsim 5000$ . For future SZ surveys such as SPT, which will cover 10% of the sky, the PDF of the SZ power spectrum can be approximated as Gaussian at  $l \gtrsim 1000$ . For Planck, the PDF of the SZ power spectrum can be approximated as Gaussian at all relevant scales.

While useful, our results should be treated with caution for a number of reasons. (1) We have assumed cluster dark matter density profiles are universal, and can be described by the NFW profile. N-body simulations show that a non-negligible fraction of clusters are not well fit by this form (Jing & Suto 2000). (2) At fixed mass, halos which are well fit by the NFW form have a range of concentrations (Bullock et al. 2001; Jing & Suto 2002). We have not accounted for this scatter. (3) We have assumed that clusters are spherical. In reality, clusters are better described as tri-axial spheroids (Jing & Suto 2002). This will cause the SZ signal of a cluster to be non-spherical (Wang & Fan 2004). These complexities will increase the variance of the distribution of  $C_\ell$ .

Of perhaps more concern is that fact that our assumption of a spherically symmetric profile leads to the unrealistic prediction that different  $l$  with the same amplitude  $|l|$  are completely correlated. On the other hand, the measured quantity is almost always a band-power averaged SZ power spectrum, where the average is over different  $l$ , so the assumption of spherical profiles should be accurate to lowest order. Nevertheless, it might be interesting to account for halo triaxiality.

Incorporating (1), (2) and (3) into our model (equations 23 and 30) is relatively straightforward. Cooray & Sheth (2002) shows how the scatter in halo concentrations can be incorporated into the halo model, and Smith, Watts & Sheth (2006) show how to incorporate the effects of halo triaxiality into models of the dark matter power spectrum. Since this is particularly straightforward for the one-halo term, it might be interesting to combine their analyses with ours. But doing so is beyond the scope of our present work.

While  $P(C)$  is important for assigning realistic errors to measurements of the SZ power spectrum, thus permitting accurate constraints on cosmological parameters, it also contains important information about cosmological and gas physics. For example, the shape of the tail at  $C > \bar{C}$  is sensitive to the number of clusters in the survey and to the gas fraction in clusters. With sufficiently large sky coverage, one can divide the survey area into many  $1 \text{ deg}^2$  patches, thus providing a direct measurement of

the SZ PDF on 1 deg<sup>2</sup> scales. Comparison with Fig. 4 then constrains cluster abundances and gas physics. A detailed analysis of how much additional information (i.e. more than is provided by the power spectrum itself) is contained in the full PDF is beyond the scope of this paper, although it certainly deserves further investigation.

It would have been nice to test our predictions with measurements from numerical simulations. However, current SZ simulations lack sufficiently large independent simulation volumes to measure the PDF reliably beyond the lowest moments. That said, we stress that the variance of the SZ power spectrum which our approach predicts is in excellent agreement with simulations (c.f. §2). This gives us confidence that our approach should at least provide a useful template for more accurate model of the SZ PDF.

The analytical approach described in this paper can be applied to several other cases. For example, it can be applied to calculate the PDF of the lensing power spectrum at high  $\ell$  straightforwardly, where the one halo term

dominates. At low  $\ell$  where two halo term becomes important or even dominant in the lensing power spectrum, this is less straightforward. Extending this approach to include the two halo term and so make predictions for the PDF of the weak lensing power spectrum is under investigation.

#### ACKNOWLEDGMENTS

We thank Houjun Mo for helpful discussions on the application of the PDF to constrain cosmology and gas physics and Oliver Zahn for useful comments. We thank the anonymous referee for useful suggestions. PJZ thanks the University of Pennsylvania astrophysics group for the hospitality where this work was initiated and finalized. PJZ is supported by the One-Hundred-Talent Program of the Chinese Academy of Science and the National Science Foundation of China grants (No. 10533030, 10543004, 10673022). RKS was supported by NASA-ADP grant NNG05GK81G.

#### REFERENCES

- Atrio-Barandela, F.; Mucket, J. P., 1999, *Astrophys. J.* , 515, 465  
Atrio-Barandela, F., Mucket, J. P. 2006, *Astrophys. J.* , 643, 1  
Bardeen, J. M.; Bond, J. R.; Kaiser, N.; Szalay, A. S., 1986, *Astrophys. J.* , 304, 15  
Birkinshaw, M. 1999, *Physical Report*, 310, 97  
Bond, J. R., et al. 2005, *Astrophys. J.* , 626, 12  
Bullock, J. S., Kolatt, T. S., Sigad, Y., Somerville, R. S., Kravtsov, A. V., Klypin, A. A., Primack, J. R., & Dekel, A. 2001, *MNRAS*, 321, 559  
Carlstrom, J. E., Holder, G. P., & Reese, E. D. 2002, *ARAA*, 40, 643  
Casas-Miranda R., Mo, H. J., Sheth, R. K., Börner G., 2002, *MNRAS*, 333, 730  
Cole, Shaun; Kaiser, Nick, 1988, *MNRAS*, 233, 637  
Cooray, A. 2001, *Phys. Rev. D* , 64, 063514  
Cooray, A., Sheth, R. K., 2002, *Phys. Rep.*, 372, 1  
da Silva, Antonio C.; Barbosa, D.; Liddle, A. R.; Thomas, P. A., 2000, *MNRAS*, 317, 37  
da Silva, A. C., Kay, S. T., Liddle, A. R., Thomas, P. A., Pearce, F. R., Barbosa, D., 2001, *Astrophys. J.* , 561, 15L  
Dawson, K. S., Holzzapfel, W. L., Carlstrom, J. E., Joy, M., LaRoque, S. J., Miller, A. D., Nagai, D, 2002, *Astrophys. J.* , 581, 86  
Dawson, K.S. et al. 2006, *astro-ph/0602413*.  
Douspis, M., Aghanim, N., & Langer, M. 2006, *A&A*, 456, 819  
Hernandez-Montegudo, C., Trac, H., Jimenez, R., & Verde, L. 2006, *astro-ph/0606172*  
Holder, G. P. 2002, *Astrophys. J.* , 578, L1  
Holder, G. P. 2006, *astro-ph/0602251*  
Hu, W., Cohn, J., *Phys. Rev. D* , 73 06301  
Jing, Y. P. 1999, *Astrophys. J.* , 515, L45  
Jing, Y. P., & Suto, Y. 2000, *Astrophys. J.* , 529, L69  
Jing, Y. P., & Suto, Y. 2002, *Astrophys. J.* , 574, 538  
Komatsu, E., Kitayama, T. 1999, *Astrophys. J.* , 526, L1  
Komatsu, E., Seljak, U., 2001, *MNRAS*, 327, 1353  
Komatsu, E., Seljak, U., 2002, *MNRAS*, 336, 1256  
Kuo, C.L. et al. 2006, *astro-ph/0611198*  
Lin, K.-Y., Woo, T.-P., Tseng, Y.-H., Lin, L., & Chiueh, T. 2004, *Astrophys. J.* , 608, L1  
Majumdar, S., 2001, *Astrophys. J.* , 555, L7  
Makino, N.; Suto, Y., 1993, *Astrophys. J.* , 405, 1  
Malyshkin, L., 2001, *Astrophys. J.* , 554, 561  
Mason, B. S., 2003, *Astrophys. J.* , 591, 540  
Mo, H. J.; White, S. D. M., 1996, *MNRAS*, 282, 347  
Molnar, S. M., Birkinshaw, M., 2000, *Astrophys. J.* , 537, 542  
Navarro, J. F., Frenk, C. S., White, S. D. M., 1996, *Astrophys. J.* , 462, 563  
Navarro, J. F., Frenk, C. S.; White, S. D. M., 1997, *Astrophys. J.* , 490, 493  
Newman, W., Newman, A.; Rephaeli, Y., 2002, *Astrophys. J.* , 575, 755  
Oh, S. P., Cooray, A., Kamionkowski, M. 2003, *MNRAS*, 342, L20  
Press, W. H., Schechter, P. L., 1974, *Astrophys. J.* , 187, 425  
Readhead, A. C. S., et al. 2004, *Astrophys. J.* , 609, 498  
Refregier, A., Komatsu, E. Spergel, D. N., Pen, U.-L., 2000, *Phys. Rev. D* , 6113001  
Refregier, A., Teyssier, R. 2002, *Phys. Rev. D* , 66, 043002  
Seljak, U., Burwell, J., Pen, U.-L., 2001, *Phys. Rev. D* , 63, 063001  
Seljak, U., Warren, M. S. 2004, *MNRAS*, 355, 129  
Sheth, R. K., Lemson, G. 1999, *MNRAS*, 304, 767  
Sheth, R. K., Tormen, G. 1999, *MNRAS*, 308, 119  
Sheth, R. K., Tormen, G. 2002, *MNRAS*, 329, 61  
Smith, R. E., Watts, P. I. R., Sheth, R. K. 2006, *MNRAS*, 365, 214  
Spergel, D. N., et al. 2003, *Astrophys. J. Suppl.*, 148, 175  
Spergel, D.N., et al. 2006, *astro-ph/0603449*  
Springel, V., White, M., Hernquist, L., 2001, *Astrophys. J.* , 549, 681  
Sunyaev, R. A., & Zeldovich, Y. B. 1972, *Comments on Astrophysics and Space Physics*, 4, 173  
Toffolatti, L., Negrello, M., González-Nuevo, J., de Zotti, G., Silva, L., Granato, G. L., & Argüeso, F. 2005, *A&A*, 438, 475  
Wang, Y.-G., & Fan, Z.-H. 2004, *Astrophys. J.* , 617, 847  
Wechsler, R. H., Bullock, J. S., Primack, J. R., Kravtsov, A. V., & Dekel, A. 2002, *Astrophys. J.* , 568, 52  
White, M., Hernquist, L., Springel, V., 2002, *Astrophys. J.* , 577, 569L  
White, M., & Majumdar, S. 2004, *Astrophys. J.* , 602, 565  
Zeldovich, Y.B., Sunyaev, R., 1969, *Ap&SS*, 4, 301  
Yoshida, N.; Sheth, Ravi K., Diaferio, A. 2001, *MNRAS*, 328, 669  
Zhang, P., Pen, U.-L., 2001, *Astrophys. J.* , 549, 18  
Zhang, P., Pen, U.-L., Wang, B., 2002, *Astrophys. J.* , 577, 555  
Zhang, P. 2004, *MNRAS*, 348, 1348  
Zhang, Y.-Y.; Wu, X.-P., 2003, *Astrophys. J.* , 583, 529  
Zhao, D. H., Jing, Y. P., Mo, H. J., Borner, G. 2003, *Astrophys. J.* , 597, L9

## APPENDIX

## SMALL SKY COVERAGE LIMIT

For surveys with very small sky coverage,  $|\exp[\int(e^{if^C} - 1)dN]| \ll 1$ . One can then Taylor expand

$$\exp \int (e^{if^C} - 1)dN \simeq 1 + \int (e^{i\bar{f}S} - 1)dN + \frac{[\int (e^{i\bar{f}S} - 1)dN]^2}{2}.$$

Inserting into equation (17) and Fourier transforming to real space gives  $P(C)$  in the Poisson limit:

$$\begin{aligned} P(C) = & (1 - \bar{N})\delta_D(C) + \int \delta_D(Cf_{\text{sky}} - S)d\bar{N} \\ & + \frac{1}{2} \left( \int \delta_D(S_1 + S_2 - Cf_{\text{sky}})d\bar{N}_1d\bar{N}_2 \right. \\ & \quad \left. - 2 \left[ \int \delta_D(Cf_{\text{sky}} - S)d\bar{N} \right] \bar{N} + \bar{N}^2 \delta_D(C) \right) \\ & + \frac{\sigma^2}{2} \left( \int \delta_D(S_1 + S_2 - Cf_{\text{sky}})b_1b_2d\bar{N}_1d\bar{N}_2 \right. \\ & \quad \left. - 2 \left[ \int \delta_D(Cf_{\text{sky}} - S)bd\bar{N} \right] \int bd\bar{N} + \left[ \int bd\bar{N} \right]^2 \delta_D(C) \right) \end{aligned}$$

Here,  $\bar{N} = \int d\bar{N}$ . Note that this expression does not rely on the assumption that  $P_\delta$  is Gaussian. One can Taylor expand equation (18) in the limit  $f_{\text{sky}} \rightarrow 0$ , perform the Fourier Transform, and verify that equation (18) does indeed agree with the above result to order  $O(\sigma^2)$ . This suggests that equation (18) should work well for all sky coverage, even though the assumption of Gaussian  $P_\delta$  breaks in the small sky coverage limit. The Poisson limit requires

$$\text{Re}(G)f_{\text{sky}} \simeq \text{Re}\left(\sum_j D_j\right) f_{\text{sky}} \ll 1 .$$

Fig. 3 shows that only for  $f_{\text{sky}} \ll 10^{-5}$ , or the sky coverage  $\ll 0.4 \text{ deg}^2$ , will the Poisson limit be reached. In reality, the above Poisson limit expression of  $P(C)$  has very limited application, because all ongoing and upcoming SZ surveys have  $f_{\text{sky}} \gg 10^{-5}$ .